International Journal of Industrial Chemistry (2018) 9:61–73
https://doi.org/10.1007/s40090-018-0135-6

RESEARCH

Ni-supported catalysts for ethanol steam reforming: effect of the solvent and metallic precursor in catalyst preparation

Alejandra C. Villagrán Olivares[1] · Manuel F. Gomez[1] · Mariana N. Barroso[1] · María C. Abello[1]

Received: 17 May 2017 / Accepted: 30 December 2017 / Published online: 19 January 2018

Abstract
Ethanol steam reforming was studied over Ni/$MgAl_2O_4$–CeO_2 catalysts. The catalysts were prepared using different impregnation media (ethanol or water) and Ni precursors (nitrate or acetate). The use of an alcoholic solution did not affect the specific surface area, but promoted the NiO formation reducible at lower temperature affecting the Ni-support interactions and the Ce^{3+}/Ce^{4+} initial ratios. All catalysts were highly active in the reforming reaction of ethanol with a high initial conversion of ethanol under more severe conditions than those commonly used in literature. The best catalytic behavior was found over the catalyst prepared from an ethanolic solution of $Ni(NO_3)_2$. This sample showed a high Ce^{3+}/Ce^{4+} ratio, an adequate interaction Ni-support and an average Ni diameter around 28 nm. This catalyst was stable under the reforming conditions used in this work: initial ethanol concentration: 9.4%, reaction temperature: 650 °C, $W/F = 49$ g min $mol^{-1}_{C_2H_5OH}$ and reaction time: 40 h. The ethanol conversion was almost complete with H_2 selectivity around 78%.

Keywords Hydrogen · Ethanol reforming · Ni/$MgAl_2O_4$–CeO_2 catalysts · Deactivation

Introduction

The climate change observed in the last few decades and its consequences have led the global society to minimize the emissions (mainly CO_2) into the environment and to decrease the dependence on fossil fuels. The use of sustainable energy sources is imperative and it is widely accepted that a carbon-free society will not be possible without a hydrogen economy [1]. The hydrogen production from ethanol steam reforming is an interesting option, because ethanol has several advantages compared with other raw materials. The most important one is its renewable origin, because it can be obtained from biomass fermentation (e.g., sugar cane, corn, lignocelluloses, etc.) [2, 3]. The ethanol has relatively high hydrogen content and its reaction with water under steam reforming conditions is able to produce 6 mol of H_2 per mole of reacted ethanol:

$$CH_3CH_2OH + 3\,H_2O \rightarrow 6\,H_2 + 2\,CO_2. \quad (1)$$

✉ María C. Abello
cabello@unsl.edu.ar

[1] Instituto de Investigaciones en Tecnología Química, INTEQUI-CONICET-UNSL, Almirante Brown 1455, 5700 San Luis, Argentina

The other important advantage is that CO_2 production slightly contributes to greenhouse effect since it is recycled through photosynthesis during the plant growth. The noble metals [4–7], nickel [8–13], cobalt [9, 14–21], etc., supported over several supports have been studied as catalysts for this reaction. Ni catalysts have been used in commercial scale in several reforming processes for more than 40 years [22], especially for its high activity to break C–C bond and its low cost compared to noble metals. The main disadvantage of Ni catalysts is related to deactivation by coke formation, sintering and inactive phase transformation. There are many studies about the carbon formation on Ni systems [13, 23–25] and a considerable effort has been focused on developing new Ni stable catalysts with an improved resistance to coke formation.

The type of metal present (base metal or noble metal) and the reaction conditions (initial ethanol concentration, water: ethanol molar ratio, temperature, etc.) affect the mechanism of carbon deposition [3]. The addition of alkaline metals, alkaline earth metals or rare earth metals has been frequently used on Ni catalysts to increase the carbon tolerance [23, 26, 27]. It has been reported that the addition of Na or K changes the surface acidity of catalyst and minimizes the ethylene formation known as coke precursor. The inhibition of carbon deposition has been also related to Ni particle sizes. Ni

particles lower than a critical size (around 10 nm [3]) and high dispersion levels could minimize the carbon deposition responsible for the irreversible deactivation or for the pressure increase in the catalytic bed [28]. Other important factor is the Ni-support interaction. Strong interactions of NiO with the support and/or Ni compound formation can hinder the formation of metallic Ni. The anchorage of Ni particles on the support could be also affected by the impregnation medium [29] and/or the Ni precursor nature [30].

The effect of the solvent used in the impregnation step has been investigated in Co-based catalysts. Song and Ozkan [29] have studied the influence of ethanol and water as impregnation media in Co/SiO_2 catalysts. The catalysts prepared in ethanol showed a significant improvement in the ethanol steam reforming reaction, ESR: higher H_2 yield, better stability and lower amount of by-products. The authors have assigned this positive effect to the presence of oxygenated carbon species which prevent sintering and exert a site blocking that suppresses the side reactions. Besides, they have suggested an "imprinting" effect that favors the surface acetate formation and provides an optimum surface geometry for the selective reactions. The impregnation with an ethanolic solution of cobalt nitrate instead of an aqueous one has also shown an improvement in the metallic dispersion in Fischer–Tropsch Co catalysts [31]. Ho and Su have reported that the presence of ethoxy groups hinder the aggregation of Co_2O_3 during its formation from the thermal decomposition of cobalt nitrate [31]. The influence of other solvents in metallic dispersion has been also reported in literature [32, 33]. Lucredio et al. [32] have investigated the effect of methanol in the preparation of Co catalysts. They observed an improvement in the ESR when Co was supported on SiO_2. However, the performance of Co/Al_2O_3 resulted to be independent of the solvent used in preparation. The influence of methanol seems to depend on support nature.

In a previous work, Ni catalysts supported on $MgAl_2O_4$–CeO_2 showed a good performance in ESR, although they suffered deactivation mainly by carbonaceous species deposition [30]. As it was mentioned, high dispersion levels of Ni could depress coke formation. Then, it is interesting to examine the interaction of ethanol as impregnation medium in preparation of $Ni/MgAl_2O_4$–CeO_2 catalysts. In this work, the solids were synthesized by wet impregnation using ethanol with different Ni precursors: $Ni(NO_3)_2$ or $Ni(CH_3COO)_2$. The catalysts were characterized by different techniques and their catalytic results in ESR were compared with those obtained using catalysts prepared in an aqueous solution.

Experimental

Catalyst preparation

$MgAl_2O_4$ support was prepared by the citrate method [26]. The sample was calcined in two steps: (1) under a N_2 flow (180 mL min^{-1}) from room temperature to 500 °C at 5° min^{-1} and 2 h at 500 °C; cooling down in N_2 flow and then, (2) in static air from room temperature to 700 °C at 5° min^{-1} and 1 h at 700 °C. The addition of Ce (5 wt%) on support was carried out by wet impregnation using an aqueous solution of $Ce(CH_3COO)_3{\cdot}xH_2O$. The solvent was removed in a rotating evaporator at 75 °C under vacuum. The sample was dried in vacuum at 100 °C overnight. The modified support was used without calcination.

Four supported catalysts with a nominal loading of 8 wt% Ni were prepared by the wet impregnation technique using an aqueous solution (w) or an ethanolic solution (e) of $Ni(NO_3)_2{\cdot}6H_2O$ (n) or $Ni(CH_3COO)_2{\cdot}4H_2O$ (a). After impregnation, the solvent was evaporated in a rotavapor at 75 °C under vacuum and then, the samples were dried at 100 °C and calcined in air at 650 °C for 3 h. The catalysts are denoted as mentioned in Table 1. Hence, Ni(n–w) indicates a Ni catalyst prepared from an aqueous solution of nickel nitrate.

Table 1 Characteristics of fresh $Ni/MgAl_2O_4$–CeO_2 catalysts

Catalyst	Ni(n–w)	Ni(a–w)	Ni(n–e)	Ni(a–e)
Ni, wt%[a]	6.37	4.89	6.10	5.48
Ce, wt%[a]	4.23	3.36	4.30	3.93
S_{BET}, $m^2\ g_{cat}^{-1}$	113	112	111	110
H_2 consumption by TPR, μmol $H_2\ g_{cat}^{-1}$	938	897	1167	1086
mol H_2/mol Ni	0.9	1.0	1.1	1.1
% *D*	2.6	4.9	3.6	0.39
Metallic surface area, $m^2\ g_{cat}^{-1}$	1.10	1.62	1.45	0.14
d_{Ni}, nm[b]	39	21	28	259

[a] wt% determined by ICP

[b] d_{Ni} (nm) = 101/% *D* [32]. S_{BET} of unmodified support = 92 m^2/g. S_{BET} of modified support without calcination = 161 m^2/g

Catalyst characterization

Chemical composition

Nickel and cerium contents were obtained with a sequential ICP spectrometer Baird ICP 2070 equipped with a monochromator [26].

BET surface area

Specific surface areas were determined by the BET method. They were measured using a Micromeritics Gemini V analyzer by adsorption of nitrogen at − 196 °C on 100 mg of a sample previously degassed at 300 °C for 16 h under flowing N_2.

X-ray diffraction

XRD patterns were recorded with a RIGAKU diffractometer using CuKα radiation ($\lambda = 0.15418$ nm) and a rate of 3° min^{-1} in the 2θ range from 10° to 70° [26].

Infrared spectroscopy

IR spectra were recorded by a Nicolet Protegè 460 infrared spectrometer, in the region 4000–250 cm^{-1} with a resolution of 4 cm^{-1}. Compressed KBr (spectroscopy quality) disks containing 1 wt% of catalyst were employed. The disks were prepared by applying a pressure of 200 kg m^{-2} for 5 min. Each spectrum was collected by co-adding of minimum 64 scans.

Temperature programmed reduction

The TPR profiles were recorded in a conventional TPR equipment [30]. Before the run, the sample was oxidized in a 50 mL min^{-1} flow of 20 vol% O_2 in He at 300 °C for 30 min. After that, helium was admitted to remove oxygen and finally, the system was cooled to 25 °C. The sample was subsequently contacted with a 50 mL min^{-1} flow of 5 vol% H_2 in N_2, heated at a rate of 10 °C min^{-1} from 25 °C to a final temperature of 700 °C and held at 700 °C for 2 h. The hydrogen consumption was determined by calibration with H_2 (5 vol%)/N_2 mixture injections.

Chemisorption of hydrogen

H_2 pulse chemisorption was carried out in a Micromeritics Autochem II 2920 instrument. The samples were reduced at 650 °C for 45 min under a H_2 (10%)/Ar (100 mL min^{-1}, 20 °C min^{-1}). Then, they were cooled down in Ar flow (100 mL min^{-1}) until 50 °C. The chemisorption was carried out by pulses of a H_2 (10%)/Ar mixture (50 mL min^{-1}) until the peak areas remained constant. The nickel dispersion, %D, was calculated from the H_2 adsorbed volume assuming the stoichiometric ratio $H_{adsorbed}$:$Ni_{surface}$ = 1 and the cross-sectional area of the nickel atom = 0.0649 nm^2 $atom^{-1}$. Spherical particles were assumed to calculate average nickel particle sizes and d_{Ni} represents the surface-weighted average crystallite diameter in nm [34].

X-ray photoelectron spectroscopy

The XPS spectra were collected with a multitechnique system (SPECS). The conditions were similar to those used in Ref. [35]. The residual pressure inside the analysis chamber was kept at values below 2×10^{-8} mbar. Ni 2p, Al 2p and Ce 3d spectra were recorded for each fresh sample. All binding energies (BE) were referred to the C 1 s peak at 284.6 eV as a consequence the BE for the Al 2p was about 74.1 eV. The samples were ex situ reduced to 650 °C in a H_2 (5%)/N_2 flow for 45 min. In addition, they were treated inside the pre-chamber in a reductive flow H_2 (5%)/Ar at 400 °C for 10 min and atmospheric pressure before the XPS measurements. The procedure for data treatment was the same as described in [35].

Thermal gravimetry

The TG-TPO analyses were carried out in a DTG-60 Shimadzu instrument. The samples were heated from room temperature to 1000 °C at 10 °C min^{-1} under an air flow (50 mL min^{-1}). The carbon amount was expressed as %C, [30].

Scanning electron microscopy and energy dispersive X-ray spectroscopy

SEM micrographs of samples after being used in reaction were obtained in a LEO 1450 VP equipped with an energy dispersive X-ray microanalyzer (EDAX Genesis 2000) [26].

Catalytic test

The ethanol steam reforming reaction was carried out in the experimental set-up described elsewhere [26]. The reactor was operated at 650 °C and atmospheric pressure. The feed to the reactor was a gas mixture of ethanol, water and inert. The molar ratio in the feed was H_2O: C_2H_5OH: inert ≈ 5:1:5 being the initial ethanol concentration around 9.4%. In all experiments, the W/F^0_{C2H5OH} was 49 g min $mol^{-1}_{C_2H_5OH}$. To observe the catalyst deactivation within a short operation time (6 h on stream), a small amount of catalyst (50 mg) without dilution in an inert material was used. For the stability test, the catalyst was diluted with SiC in a weight ratio

1:1. Before reforming experiments, the catalyst was in situ reduced in H_2 (5%)/N_2 flow at 650 °C for 45 min. The reactants and reaction products were analyzed online by gas chromatography. Ethanol conversion ($X_{C_2H_5OH}$), selectivity to carbon products (S_i) and the hydrogen yield (Y_{H_2}) were estimated as described elsewhere [26]. The selectivity to H_2 was calculated taking into account that 6 mol of H_2 represents 100% of selectivity (Eq. 1).

Results and discussion

Characterization of fresh catalyst

The chemical composition determined by ICP spectroscopy and the specific surface areas for calcined catalysts are shown in Table 1. The average Ni and Ce compositions are 6 and 4 wt%, respectively. The use of hydrated reactives in the preparation could explain that Ni and Ce compositions are lower than the nominal ones. The BET values are similar (110–113 $m^2\ g^{-1}$) and quite high after the thermal treatment (650 °C for 3 h), regardless of the solvent or the precursor used for Ni impregnation.

The diffraction patterns of fresh samples shown in Fig. 1 reveal the presence of $MgAl_2O_4$ (2θ = 19.03°, 31.3°, 36.8°, 44.8°, 55.6°, 59.4°, 65.2°, JCPDS-21-1152), CeO_2 (2θ = 28.5°, 47.5°, 56.3°, JCPDS 30-0394) and NiO (2θ = 43.3°, 37.3°, 62.9°, JCPDS-4-835). The particle sizes of NiO could be inferred from XRD. From the broadening of peaks and the Scherrer equation ($2\theta = 43.3°$), the NiO particle size follows the order of Ni(a–e) (d_{NiO} = 17 nm) > Ni(n–e) (d_{NiO} = 11 nm) > Ni(n–w) (d_{NiO} = 9 nm) > Ni(a–w) (d_{NiO} = 7 nm). They are more affected by the impregnation medium than by precursor salt. These differences could affect the catalytic activity in ESR and the carbon accumulation rate [36, 37].

The reduction profiles are presented in Fig. 2. With the exception of Ni(n–e), the TPR profiles show two well-defined reduction peaks. The small peak (α peak) at low temperature could be assigned to Ni^{2+} species weakly interacted with the $MgAl_2O_4$, to Ni^{2+} interacted with CeO_2 particles and to the surface reduction of Ce^{4+} [38–40]. From thermodynamics bulk CeO_2 is reduced to Ce_2O_3 at high temperature (1300 °C, [41]). However, the reduction behavior of ceria has been reported to dramatically change in the presence of a metal. Recently, Löfberg et al. have reported TPR results on Ni/CeO_2 catalysts and these authors have also attributed the reduction peak around 270 °C to the presence of Ni species in very small NiO crystallites, Ni species in strong interaction with Ce species at the NiO–CeO_2 interface and/or in a Ce–Ni–O solid solution [40]. In our case, there is no evidence of solid solution formation, the presence of a strong interaction between NiO and CeO_2 cannot be ruled out. The β peak at high temperature that was attributed to the reduction of Ni^{2+} species strongly interacted with $MgAl_2O_4$ and surface Ni spinel-like species. A surface Ni compound species related to Ni strongly interacting with the Mg spinel as a "Ni aluminate" could be formed. This "Ni aluminate" is suggested to be different from pure $NiAl_2O_4$ [42]. In fact, a XPS signal of Ni^{2+} near to that attributed to pure Ni spinel was clearly observed indicating this interaction (see further). The TPR profiles for Ni(n–w) and Ni(a–w) do not show significant differences neither in the maximum temperature nor in H_2 consumption, Table 1. These results suggest that similar species were formed on the surface when the impregnation medium is water regardless of the Ni precursor. On the contrary, those prepared with an ethanol solution showed

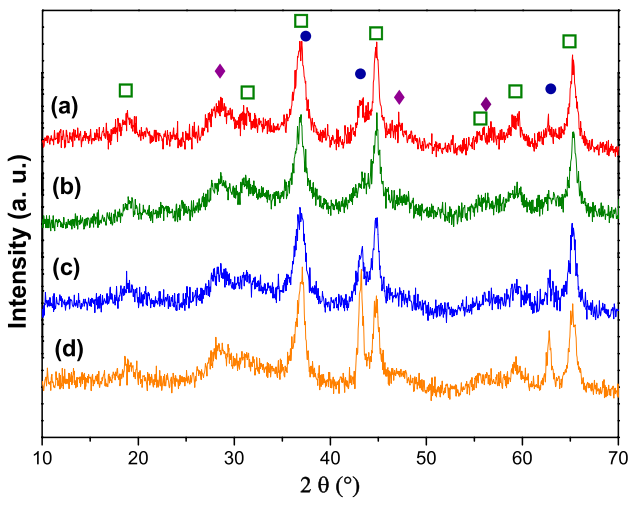

Fig. 1 Diffraction patterns of fresh catalysts. (a) Ni(n–w); (b) Ni(a–w); (c) Ni(n–e) and (d) Ni(a–e). Dark green open square: $MgAl_2O_4$, purple filled diamond: CeO_2, navy blue filled circle: NiO

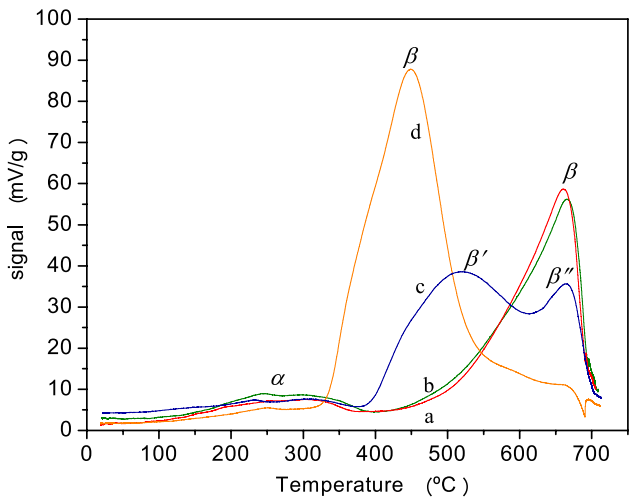

Fig. 2 Temperature programmed reduction profiles of the catalysts. (a) Ni(n–w); (b) Ni(a–w); (c) Ni(n–e) and (d) Ni(a–e)

a marked improvement in reducibility without significant changes in the extent of reduction. An improvement in reducibility was also reported for Co/CeO_2 catalysts synthesized using ethanol as an impregnation solvent [29]. For Ni(a–e) sample, the α peak decreases its intensity without changes in the maximum temperature. This could indicate an inhibition in the surface reduction of ceria. This inhibition could be associated with the blocking of reduction sites arising to ethoxy groups of solvent and/or to acetate groups of Ni precursor. The β peak (at 450 °C) is shifted in 200 °C at lower temperatures and could be assigned to the reduction of large NiO particles observed by XRD. The profile for Ni(n–e) is more complex. The peak at a high temperature for Ni(n–e) is clearly split, β′ (520 °C) and β″ (665 °C), suggesting that Ni species (NiO and surface Ni spinel) have different interaction extent with support.

Carbon contamination in fresh catalysts was confirmed by IR spectroscopy, Fig. 3. Bands between 1600 and 1400 cm^{-1} clearly reveals the presence of organic remains. Organic species remains on $MgAl_2O_4$ after calcination at 700 °C (curve e). The intense bands at 1573, 1435 and 1344 cm^{-1} for $MgAl_2O_4$–CeO_2 (curve f) without calcination correspond to υ_{as}(COO), υ_s(COO) and CH_3 bending of acetate groups (the support was modified by using $Ce(CH_3COO)_3$) [43]. In all samples, multiples bands in the COO band region are observed (1640, 1512, 1400 and 1260 cm^{-1}) and they are more intense for samples prepared from $Ni(CH_3COO)_2$. The organic remains left on the Ni(a–w) and Ni(a–e) catalyst surface are similar and stable enough to withstand calcination at 650 °C for 3 h and they could certainly contribute to the early deactivation observed in ESR reforming on these catalysts.

The XRD patterns of reduced samples after TPR reveal the presence of $MgAl_2O_4$ and CeO_2 without significant changes, Fig. 4. The NiO peaks are not detected whereas that corresponding to Ni^0 at $2\theta = 51.8°$ (JCPDS-04-0850) is clearly observed. The peak at 44.4° would be overlapped with that of $MgAl_2O_4$. From the broadening peak at $2\theta = 51.8°$, the particle metallic size are lower for Ni(n–w), Ni(a–w) and Ni(n–e) samples.

The dispersion values, % *D*, estimated by chemisorption of H_2 are presented in Table 1. This technique is not completely adequate for Ni dispersion determination due to the presence of ceria which is also reduced in the first steps of the procedure. Taking into account that the ceria reduction occurs almost in the same extent (see TPR, Fig. 2), the dispersion values could be compared. The % *D* values for the samples except to Ni(a–e) are between 2.6 and 4.9%, leading to average d_{Ni} of 39–21 nm. These values follow the same trend of those obtained by XRD. However, Ni particle sizes predicted by H_2 chemisorption are around twice those from XRD. In fresh samples, several Ni^{2+} species are present on the support: dispersed Ni^{2+} species, NiO particles and surface spinel-like species (different to $NiAl_2O_4$). The particle size of Ni estimated by Scherrer only corresponds to Ni detected by XRD. Ni^0 becoming from the surface spinel-like species observed by XPS (see

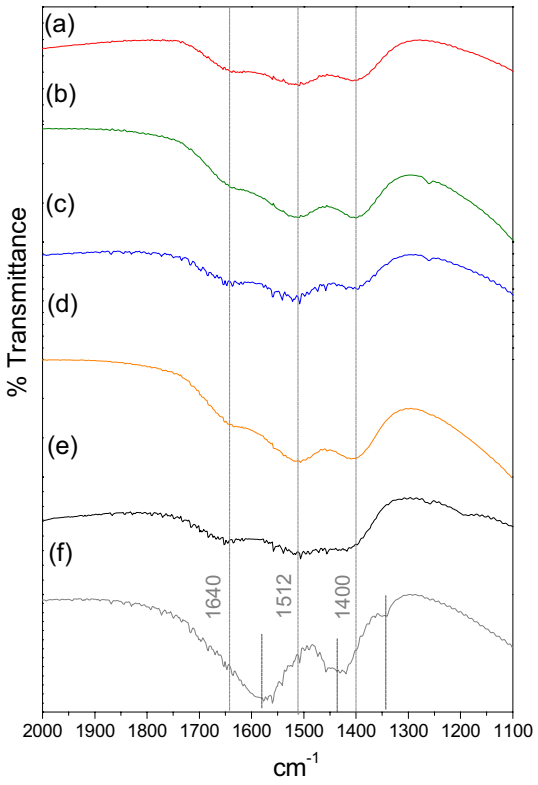

Fig. 3 IR spectra of fresh catalysts: (a) Ni(n–w); (b) Ni(a–w); (c) Ni(n–e) and (d) Ni(a–e); and (e) $MgAl_2O_4$ and (f) $MgAl_2O_4$–CeO_2

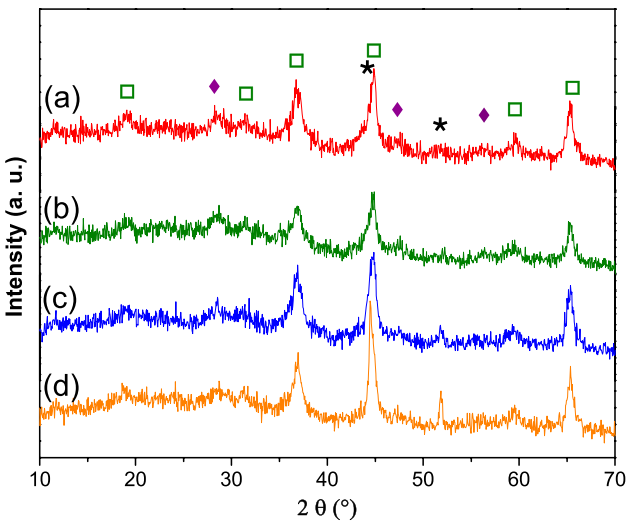

Fig. 4 Diffraction patterns of reduced catalysts. (a) Ni(n–w); (b) Ni(a–w); (c) Ni(n–e) and (d) Ni(a–e). dark green open square: $MgAl_2O_4$, purple filled diamond: CeO_2 and *: Ni^0

further) and/or from amorphous NiO would be undedectable by XRD. The dispersion for Ni(a–e), 0.39%, was markedly lower, probably related to its reduction behavior. The TPR profile of this sample presented a maximum at 450, 200 °C below the others, Fig. 2. In the chemisorption experiments, the samples were in situ reduced at 650 °C (it is the temperature at which the major fraction of Ni^{2+} of the other samples was reduced). Therefore, the metallic particles generated at 450 °C have different ages than those generated at 650 °C and have a higher possibility to be sintered. This could explain the differences in dispersion and in the behavior against carbon deposition. The catalyst is reduced in $H_2(5\%)/N_2$ flow at 650 °C for 45 min before carrying out the ESR catalytic experiments. As a consequence, the particle size of metallic nickel over Ni(a–e) would be seven to twelve times as large as the other catalytic systems.

The redox properties of catalysts were analyzed by XPS. As it was mentioned, first the samples were ex situ reduced at 650° during 45 min (to simulate its surface state at the beginning of reaction) and then, in the XPS pre-chamber at 400 °C for 10 min (to reduce NiO_x species formed during air exposure of the sample). The XP spectrum of Ni 2p presented peaks at binding energies corresponding to Ni^0 and Ni^{2+}, Fig. 5-I and Table 2. The presence of Ni^{2+} could be indicating that the additional in situ reduction at 400 °C for 10 min in the pre-chamber was insufficient to clean the surface oxidation due to the handling of samples or the reduction treatment was incomplete. The in situ reduction at 650 °C cannot be made in the XPS equipment used in this work. The XP spectrum for Ce 3d, Fig. 5-II, exhibited peaks at 879.8–880.1, 882.2–882.3, 885.2–885.3, 887.7–887.9, 897.5–898.0 eV corresponding to Ce 3d5/2 which could be assigned to Ce^{+4} (v, v'', v''') and Ce^{+3} ($v°$, v') [35].

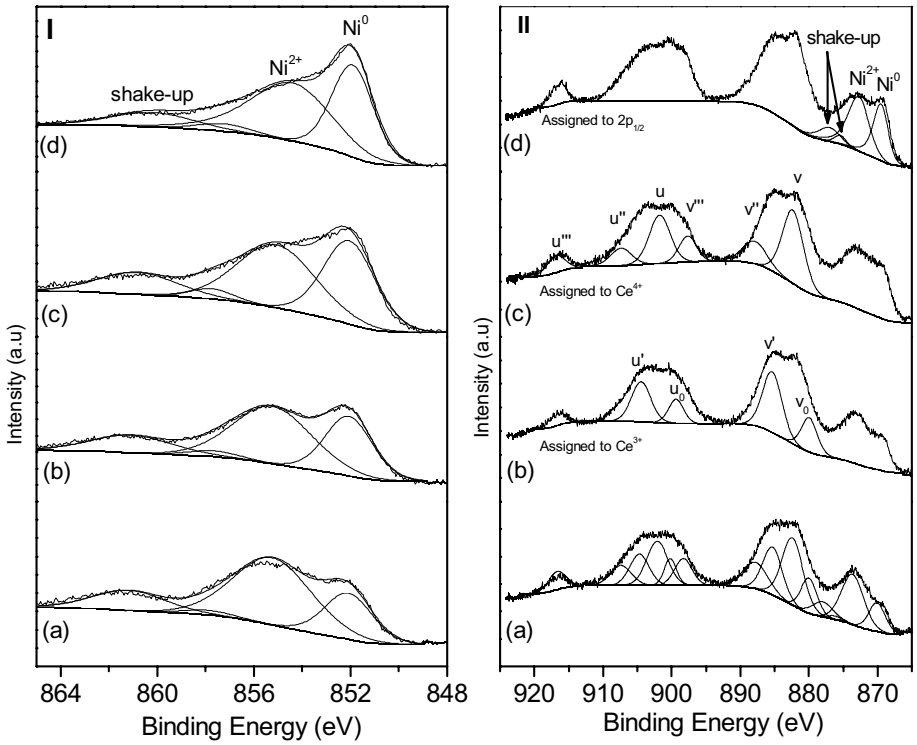

Fig. 5 X-ray photoelectron spectra of (a) Ni(n–w), (b) Ni(a–w), (c) Ni(n–e) and (d) Ni(a–e) in: **I** the Ni 2p region and (**II**) the Ce 3d region, peak assignments for Ce^{3+}, Ce^{4+} and Ni $2p_{1/2}$

Table 2 XPS results for reduced catalysts

Catalyst	Binding energy, eV									Surface ratio		
	Ni 2p3/2				Ce 3d5/2					Ni^0/Ni	Ce^{3+}/Ce^{4+}	Ni/Ce + Ni
	Ni^0	NiO	$NiAl_2O_4$	Sat.NiO	v'	v	v^0	v''	v'''			
Ni(n–w)	852.2	855.4	858.0	861.4	879.8	882.2	885.2	887.7	898.0	0.25	0.53	0.68
Ni(a–w)	852.1	855.3	857.7	861.1	880.1	882.3	885.3	887.9	897.6	0.30	0.74	0.64
Ni(n–e)	852.1	855.1	857.7	860.8	880.1	882.3	885.3	887.9	897.6	0.38	0.70	0.69
Ni(a–e)	851.9	854.4	857.2	860.2	879.9	882.2	885.2	887.8	897.5	0.37	0.54	0.67

The Ni/(Ce + Ni) surface ratios show non-significant changes, between 0.64 and 0.69, Table 2. The Ce^{3+}/Ce^{4+} ratio was determined from curve fitting and integration of the Ce 3d region. There is not a clear dependence with the precursor nature or the impregnation medium. The Ce^{3+}/Ce^{4+} ratio for Ni(a–e) was lower than the value for Ni(n–e), 0.54 against 0.7; whereas the Ce^{3+}/Ce^{4+} ratio for Ni(a–w) was higher than the one corresponding to Ni(n–w), 0.74 against 0.53. The presence of the redox couple Ce^{3+}/Ce^{4+} is crucial to increase the carbon tolerance [35]. The Ni^0/Ni ratios were higher for the samples prepared in presence of ethanol.

Catalytic results in ethanol steam reforming

Catalytic results are shown in Fig. 6. High ethanol conversions were reached from the beginning of the reaction. The samples prepared from acetate precursor showed a faster deactivation, in agreement with previous results [44, 45]. The Ni(a–e) catalyst exhibited a marked loss of conversion from 100 to 72% after 350 min in time on stream. The loss of conversion was lower for catalysts prepared from $Ni(NO_3)_2$ regardless of impregnation solvent.

As regards to performance to H_2, the catalysts prepared in aqueous medium presented higher values than those prepared in an ethanolic medium. The Ni(n–w) catalyst showed an initial yield close to 5.2 mol H_2/mol C_2H_5OH decreasing to 4.5. Furthermore, this catalyst showed the highest selectivity (an average of 80% value). For the system Ni(a–w), H_2 yield also decreased from 4.5 to 4 mol H_2/mol C_2H_5OH. However, for Ni(n–e), the H_2 yield was kept constant near to 4.2 mol H_2/mol C_2H_5OH. The lowest value of H_2 yield was 3 mol H_2/mol C_2H_5OH for Ni(a–e) catalyst due to the formation of C_2H_4O ($S_{C_2H_4O}$ ~ 14%), CH_3COCH_3 ($S_{CH_3COCH_3}$ ~ 9%) and C_2H_4 ($S_{C_2H_4}$ = 3.6%, known as coke precursor). The CH_4 selectivity for all catalysts was near to 3%. The carbon balances were relatively low indicating a continuous carbon deposition on the catalysts.

The Ni particles size is substantially higher on Ni(a–e) which could explain the different catalytic behaviors. The

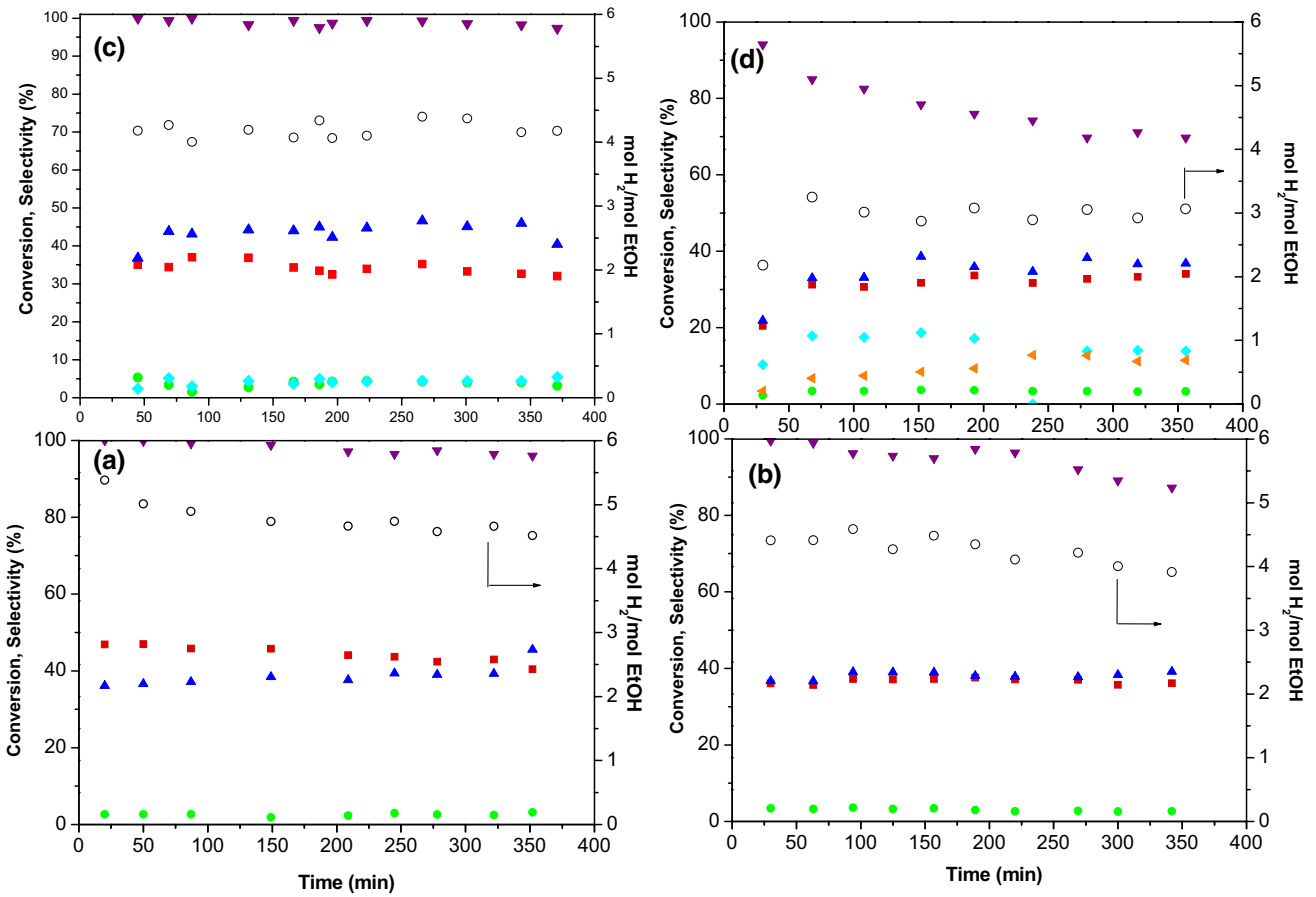

Fig. 6 Ethanol conversion and products distribution over **a** Ni(n–w), **b** Ni(a–w), **c** Ni(n–e) and **d** Ni(a–e) as a function of time on stream brown filled downward triangle: ethanol conversion; o: mol H_2/mol C_2H_5OH; selectivity to blue filled upward triangle CO_2, red filled square CO, light green filled circle CH_4 and aqua blue filled diamond C_2H_4O. Initial ethanol concentration: 9.4%, reaction temperature: 650 °C, W/F = 49 g min $mol^{-1}_{C_2H_5OH}$

simultaneous presence of ethoxy groups in the solvent and acetate groups from Ni precursor during the thermal decomposition could also affect the morphology of Ni particles and change the Ni–CeO_2 interactions. The difference in size and shape of Ni particles with the different types of lattice planes exposed has been reported to have a significant effect on the ESR reaction rate and carbon deposition [46, 47]. Besides, it cannot be ruled out that the organic remains could be blocking the active sites for selective reactions. This hypothesis cannot be conclusively confirmed based on the available characterization data.

All catalysts were active in the reforming reaction of ethanol with a high initial conversion of ethanol under more severe conditions than those commonly used in literature (inlet ethanol concentration around 10% and 50 mg of catalyst without dilution to observe the catalyst deactivation within a short operation time). As it is known that the activity, selectivity and stability are strongly affected by the reaction conditions (temperature, feed composition, residence time, etc.) and the nature of catalyst. Recent catalytic results in this reaction over similar Ni catalysts are reported in Table 3. The differences observed with the present results could be explained from the different operating conditions and also the nature of catalyst. The carbon deposition rate could be an indicator of performance in similar operation conditions (see further).

Table 3 Catalytic results in ESR over Ni-based catalysts

Catalytic system	Operating conditions in ESR	$X_{C_2H_5OH}$	Main products	Carbon deposition	References
NiMAl (M: Mg, Ca, Zn) and NiMgN (N: La, Ce) With Ni loadings around 7 wt% (A) NiMgAl, (B) NiMgCe	Catalyst weight = 315 mg Reaction temperature = 600 °C Atmospheric pressure Nitrogen flow = 30 N mL/min H_2O:C_2H_5OH molar ratio = 3.7 Flow rate = 0.075 mL/min W/F = 12.7 h^{-1}	(A) 100% TOS: 8 h (B)From 100 to 60% TOS: 8 h	Selectivity (A) H_2: 78%, CO_2: 46%, CO: 27%, CH_4: 26%, CH_3CHO: 2% (B) H_2: 82%, CO_2: 58%, CO: 14%; CH_4: 13%, CH_3CHO: 15%	(A) 1583 mg C/g_{cat} h (B) 41 mg C/g_{cat} h Coke amount: NiMgAl ≫ NiZnAl > NiCaAl > NiMgLa > NiMgCe	[48]
Ni/10%)/MgO–CeO_2 Mg molar fraction in the support 10 mol %	Catalyst weight: 200 mg mixed with 1 mL quartz particles Reaction temperature = 400 °C H_2O:C_2H_5OH molar ratio = 8 $W/F_{C_2H_5OH}$ = 33 g h/mol	100% TOS: 10 h	Selectivity H_2: 65% CO: 2% CO_2: 60% CH_4 :40% C_2H_4 + C_2H_6 + CH_3CHO + CH_3C-OCH_3: 0.25%	15 mg C/g_{cat} h	[49]
Ni(8.2%)/$MgAl_2O_4$	Catalyst weight = 500 mg Reaction temperature = 590 °C H_2O:C_2H_5OH molar ratio = 6 Inlet ethanol concentration = 3, 3.3% Flow rate = 1600 N mL/min	From 83 to 75% TOS = 4 h	Selectivity H_2 = 69% CO_2/CO molar ratio = 3.7	28 mg C/g_{cat} h	[50]
Ni–Ce–Mg–Al Ni(5.5%), Ce(10.5%)	Catalyst weight = 3 Reaction temperature = 540 °C H_2O:C_2H_5OH molar ratio = 6 Flow rate = 0.02 mL/min Special time = 22.04 kg_{cat} h/$kmol_{feed\ ethanol}$	≈ 96% TOS: 10 h	Yield in mol/mol_{C2H5OH} H_2: ~ 2.5 CO_2: ~ 0.5 CO: ~ 1 CH_4: < 0.3	16.5 mg C/g_{cat} h	[51]
Ni (7%)/MgO–CeO_2	Catalyst weight = 30 mg Reaction temperature = 600 °C H_2O:C_2H_5OH molar ratio = 6 (54 and 9% of water and ethanol in the inlet feed, respectively) Liquid feed flow = 1 mL/h to 15 mL/h GHSV = 4895 mL/g_{cat}/h W/F = 0.735 g s/mL	~100% TOS = 18 h	Selectivity H_2: ~ 70% CO_2: ~ 20% CO: ~ 10% CH_4: < 5%	13.9 mg C/g_{cat} h	[52]

Characterization of used catalysts in ethanol steam reforming

The presence of carbon deposits was detected in all the used catalysts. Characterizations of used catalysts were carried out with the aim to determine types and amounts of deposited carbon.

The diffraction patterns of used catalysts are shown in Fig. 7. Non-significant changes are observed in $MgAl_2O_4$ and CeO_2. The presence of Ni^0 is clearly detected by the characteristic peak at $2\theta = 51.8°$ indicating that the catalyst is kept activated under the reaction conditions. The patterns also reveal a peak at $2\theta \approx 43°$ which could be assigned to NiO which appears very evident in the pattern of Ni(a–e). This peak could be also assigned to MgO, due to the high similarity with the NiO XRD pattern. Since this peak does not appear in the XRD of reduced samples, Fig. 4, it could be inferred that it mainly corresponds to NiO. The presence of NiO can be explained if a fraction of metallic nickel is reoxidized under reforming conditions induced by the organic remains from preparation. The oxidation by H_2O cannot be discarded. The peak of NiO is weak in the case of Ni(n–e). The intense peak in Ni(a–e) catalyst suggests a higher amount of this phase and its presence contributes to a major deactivation. Hou et al. [53] have reported similar results in the methane autothermal reforming.

For all the used catalysts, a peak corresponding to graphitic carbon at $2\theta = 26.4°$ is also observed. The intensity of this peak follows the order of Ni(a–e) > Ni(a–w) > Ni (n–w) ≈ Ni(n–e) in a reasonable agreement with TPO-TG results (see forward). This type of carbon has been reported on Ni catalysts supported on $MgAl_2O_4$ modified by CeO_2 or ZrO_2 [30, 54].

The carbon deposition on the used samples was also studied by TG-TPO analysis in air, Fig. 8. In all the cases, a mass loss was observed between 520 and 700 °C and it was attributed to the carbon combustion [55, 56]. The TPO profiles displayed one peak at a high burning temperature (between 613° and 645 °C, Table 4) suggesting a high extent of carbon deposit graphitization [57, 58] mainly filaments or carbon nanotubes. The carbon amounts are shown in Table 4. A great amount of carbon (105%) was determined on Ni(a–e) catalyst in agreement with its high particle size (XRD and H_2 chemisorption), its minor Ni-support interaction (TPR) and the low Ce^{3+}/Ce^{4+} ratio (XPS). Comparing the carbon deposition rates expressed as mg C g_{cat}^{-1} h^{-1} (Tables 3, 4), the observed rate over Ni(n–e) is markedly lower. This catalyst seems to be a promising system for ESR.

Taking into account the %C and Ni diameter, it is clear the importance of controlling the ensemble size to minimize carbon formation. The carbon amounts for Ni(a–w)

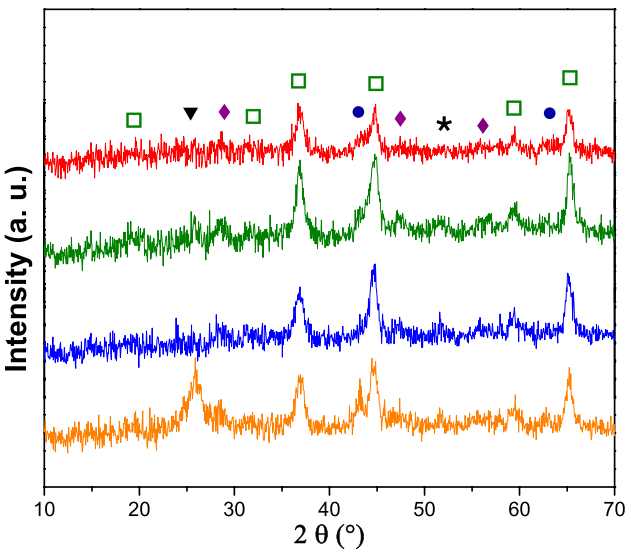

Fig. 7 Diffraction patterns of catalysts after being used in ESR. (a) Ni(n–w); (b) Ni(a–w); (c) Ni(n–e) and (d) Ni(a–e). dark green open square: $MgAl_2O_4$, purple filled diamond: CeO_2, navy blue filled circle: NiO, *: Ni^0 and black filled downward triangle: C

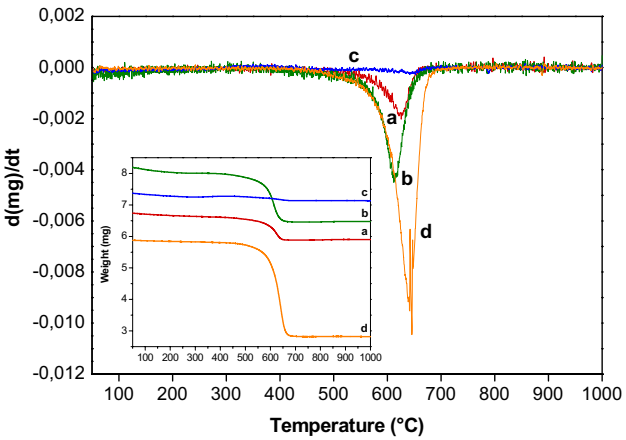

Fig. 8 Weight loss (inserted) and its TGA derivative for used catalysts in ethanol steam reforming. (a) Ni(n–w); (b) Ni(a–w); (c) Ni(n–e) and (d) Ni(a–e)

Table 4 Carbon amounts on used $Ni/MgAl_2O_4$–CeO_2 catalysts in ESR after 6 h run

Sample	TPO-TG			EDX result	
	% *C*	$T_{burning}$ (°C)	C rate ($mgCg_{cat}^{-1}h^{-1}$)	% *C* Zone A	% *C* Zone B
Ni(n–w)	14	623	23	45	n.d
Ni(a–w)	27	613	45	65	3.5
Ni(n–e)	3	645	5	57	5.3
Ni(a–e)	105	640	175	81	11.2

n.d not determined

and Ni(n–w) were 27 and 14%, respectively. The lowest carbon amount (3%) corresponded to Ni(n–e), although the Ni particle size was higher (28 nm) than the critical size (10 nm, [3]) and related probably to its reduction behavior and to the high Ce^{3+}/Ce^{4+} value. Besides, this catalyst showed a very weak XRD peak at $2\theta = 43°$. These evidences could explain the major tolerance to carbon deposition.

The SEM micrographs and EDX results of the used catalysts are shown in Fig. 9 and Table 4, respectively. The results shown in Fig. 9 reveal that carbon deposition is clearly not homogeneous. Two different regions A and B are observed. In the A zone, an abundant filament formation was

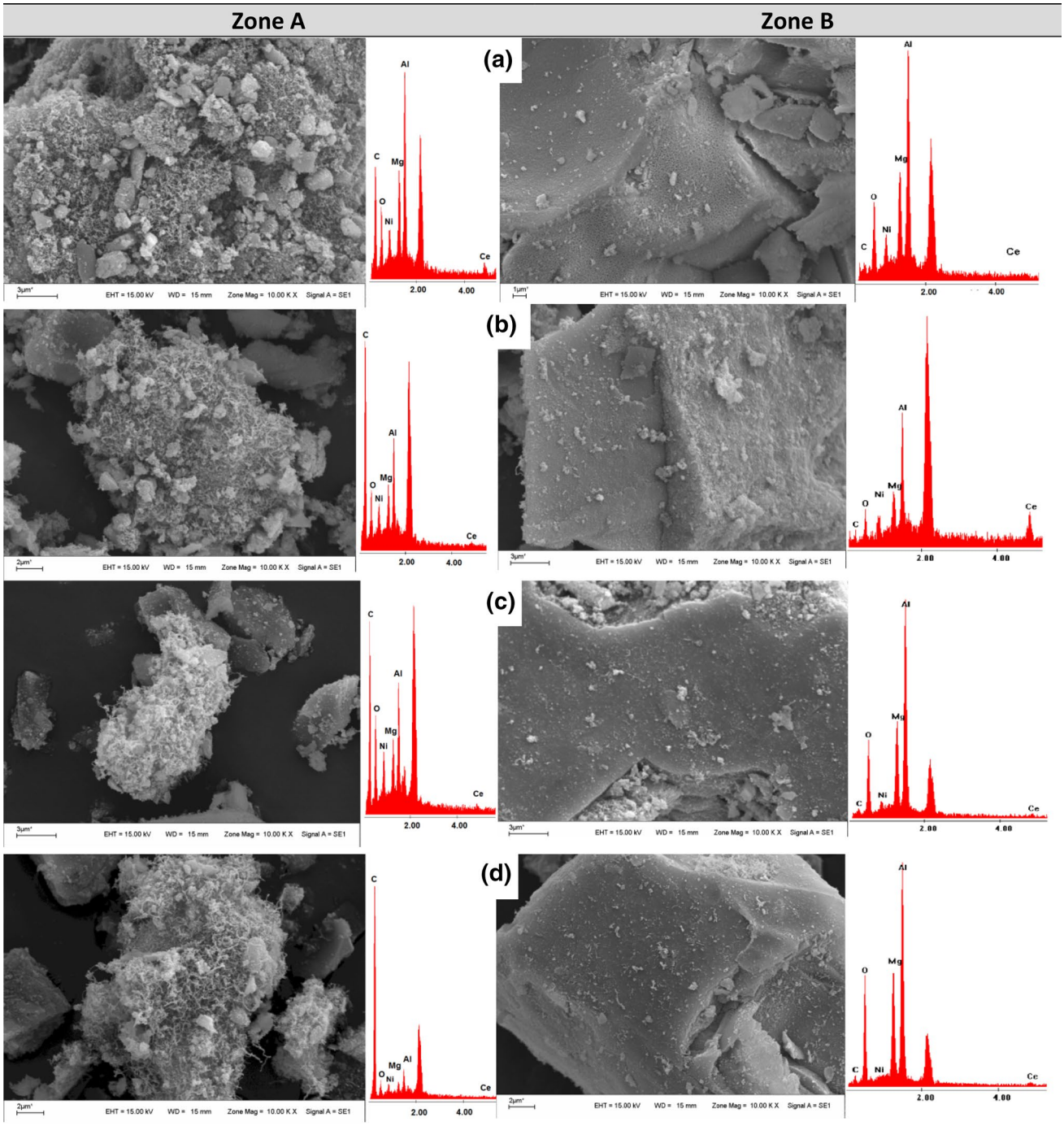

Fig. 9 SEM micrographs of used catalysts in ESR. (a) Ni(n–w); (b) Ni(a–w); (c) Ni(n–e) and (d) Ni(a–e)

detected in all the samples and Ni and Ce signals were also observed by EDX. It could be inferred that the metallic Ni is exposed at the tip of fibers and that the Ce could be interacting with a fraction of Ni particles more than with $MgAl_2O_4$. The amount of carbonaceous deposits is markedly lower in the B zone and a fraction of the support is coke free. The %C values, except for Ni(n–e), satisfactorily agree with the trend observed by TG-TPO and XRD, Table 4. The high %C value estimated for Ni(n–e) is due to the EDX analysis that was carried out on the A zone where the amount of filaments was abundant and it does not represent the whole carbon deposit.

Stability test

From a catalytic result analysis, Ni(n–e) and Ni(n–w) samples showed good catalytic performances in ESR. However, in spite of the good hydrogen selectivity, the system Ni(n–w) showed a high formation to CO, a moderate amount of carbon after 6 h in reaction, a low surface Ce^{3+}/Ce^{4+} ratio (0.53), a lower reducibility and a high Ni particle size (39 nm). Although Ni(a–w) sample also showed good surface properties (Ce^{3+}/Ce^{4+}= 0.74 and d_{Ni} = 21 nm) similar to those of Ni(n–e), the extent of reduction was the lowest one (Table 1) and a loss of conversion was observed to 250 min of time on stream. The formation of different graphitic structures could also be affected by the presence of organic remains. This behavior is not clear enough at this moment. Wang and Lu have determined that carbon deposits on catalysts prepared from nitrate precursor were predominately formed by –C–C– graphitic structures, but inactive –CO–C– species were formed on catalysts prepared from organic precursor which leading to more severe deactivation [45].Similar results were found over $Ni/ZnAl_2O_4$–CeO_2 catalysts [44].

The Ni(n–e) catalyst was chosen to study the stability. This long-time run was carried out in the same reforming conditions indicated in the experimental part with an intermediate overnight stay at room temperature in He flow. An increase of temperature due to the endothermic effect of reaction ($\Delta H^0_{650°C}$ = 206.4 kJ mol^{-1}, calculated using HSC Chemistry for Windows [41]) was observed when the feed was stopped. Then, the catalyst (50 mg) was diluted with SiC in a weight ratio of 1:1. Thus, the strong variation of temperature when the feed was stopped was avoided and the thermally induced changes in catalytic surface were minimized. Ni(n–e) catalyst operated without problems during 40 h. In Fig. 10, the ethanol conversion and products distribution are shown. The catalytic results reveal a very good behavior in ESR with an increase in the H_2 selectivity (78%) at the expense of decreasing the selectivity of C_2H_4O and the CO/CO_2 molar ratio. The dilution improved the isothermal reactor condition and it could be affecting the reforming/decomposition of acetaldehyde and water

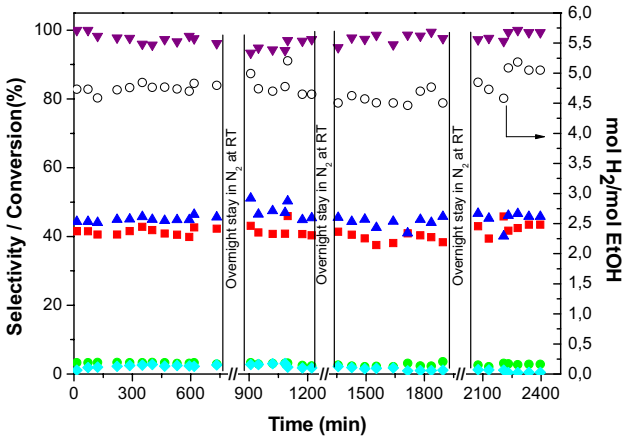

Fig. 10 Stability test over Ni(n–e) catalyst. Brown filled downward triangle: ethanol conversion; o: mol H_2/mol C_2H_5OH; selectivity to blue filled upward triangle CO_2, red filled square CO, light green filled circle CH_4 and aqua blue filled diamond C_2H_4O. Initial ethanol concentration: 9.4%, reaction temperature: 650 °C, W/F = 49 g min $mol^{-1}_{C_2H_5OH}$

gas shift reactions, known contributions during the whole process. No sign of deactivation was observed, but carbon was determined by TPO-TG. The maximum combustion temperature was 690 °C and the accumulation rate of C was 17.7 mg C g^{-1}_{cat} h^{-1}. The coke formation is still important and may lead to a considerable deactivation in higher long-term operation. Regeneration strategies should be studied and optimized taking into account whether the reforming reactor will be used for mobile or stationary applications.

Conclusions

Ni catalysts supported over $MgAl_2O_4$–CeO_2 were prepared using different impregnation media (ethanol or water) and Ni precursors (nitrate or acetate). The use of an alcoholic solution did not affect the specific surface area, but promoted the NiO formation reducible at lower temperature affecting the Ni-support interactions and the Ce^{3+}/Ce^{4+} initial ratios.

All the catalysts were highly active in the reforming reaction of ethanol with a high initial conversion of ethanol under more severe conditions than those commonly used in literature. The catalysts obtained from Ni acetate suffered deactivation from the beginning of reaction regardless of the solvent used in the impregnation step. The Ni(n–w) system showed high selectivity to H_2, the highest CO formation and an amount of deposited carbon of 14% after 6 h in reaction. However, the system Ni(n–e) was better in terms of resistance to carbon deposition with a similar selectivity to H_2. This behavior was associated with the high Ce^{3+}/Ce^{4+} initial ratio and an adequate Ni-support interaction. These

properties of Ni(n–e) increased the tolerance to carbon despite the Ni particles being relatively large.

Acknowledgements Financial supports are acknowledged to CONICET, ANPCyT and Universidad Nacional de San Luis. The authors are grateful to ANPCyT for Grant PME 8-2003 to finance the purchase of the UHV Multi Analysis System. The authors thank Ana Tarditi (INCAPE, Santa Fe, Argentina) for her assistance in XPS determinations.

References

1. Dincer I, Acar C (2015) Review and evaluation of hydrogen production methods for better sustainability. Int J Hydrogen Energy 40:11094–11111
2. Laborde M (2006) Producción y Purificación de hidrógeno a partir de bioetanol y su aplicación en pilas de combustibles. Ed. CYTED, Buenos Aires
3. Mattos LV, Jacobs G, Davis BH, Noronha FB (2012) Production of hydrogen from ethanol: review of reaction mechanism and catalyst deactivation. Chem Rev 112:4094–4123
4. Auprêtre F, Descorme C, Duprez D (2002) Bio-ethanol catalytic steam reforming over supported metal catalysts. Catal Commun 3:263–267
5. Coronel L, Múnera JF, Tarditi AM, Moreno MS, Cornaglia LM (2014) Hydrogen production by ethanol steam reforming over Rh nanoparticles supported on lanthana/silica system. Appl Catal B Environ 160–161:254–266
6. Carbajal-Ramos IA, Gomez MF, Condó AM, Bengió S, Andrade-Gamboa JJ, Abello MC, Gennari FC (2016) Catalytic behavior of Ru supported on $Ce_{0.8}Zr_{0.2}O_2$ for hydrogen production. Appl Catal B Environ 181:58–70
7. Bilal M, Jackson SD (2017) Ethanol steam reforming over Pt/Al_2O_3 and Rh/Al_2O_3 catalysts: the effect of impurities on selectivity and catalyst deactivation. Appl Catal A Gen 529:98–107
8. Campos CH, Osorio-Vargas P, Flores-González N, Fierro JLG, Reyes P (2016) Effect of Ni loading on lanthanide (La and Ce) promoted γ-Al_2O_3 catalysts applied to ethanol steam reforming. Catal Lett 146:433–441
9. Kubacka A, Fernandez Garcia M, Martinez Arias A (2016) Catalytic hydrogen production through WGS or steam reforming of alcohols over Cu, Ni and Co catalysts. Appl Catal A Gen 518:2–17
10. Szijjarto GP, Paszti Z, Sajo I, Erdohelyi A, Radnoczi G, Tompos A (2013) Nature of the active site in Ni/$MgAl_2O_4$-based catalysts designed for steam reforming of ethanol. J Catal 305:290–306
11. Marinho ALA, Rabelo-Neto RC, Noronha FB, Mattos LV (2016) Steam reforming of ethanol over Ni-based catalysts obtained from $LaNiO_3$ and $LaNiO_3$/$CeSiO_2$ perovskie-type oxides for the production of hydrogen. Appl Catal A Gen 520:53–64
12. Llera I, Mas V, Bergamini ML, Laborde M, Amadeo N (2012) Bio-ethanol steam reforming on Ni based catalyst. Kinetic study. Chem Eng Sci 71:356–366
13. Montero C, Ochoa A, Castaño P, Bilbao J, Gayubo AG (2015) Monitoring Ni^0 and coke evolution during the deactivation of a Ni/La_2O_3–αAl_2O_3 catalyst in ethanol steam reforming in a fluidized bed. J Catal 331:181–192
14. Song H, Zhang L, Watson R, Braden D, Ozkan U (2007) Investigation of bio-ethanol steam reforming over cobalt-based catalysts. Catal Today 129:346–354
15. Lin S-Y, Kim DH, Ha SY (2009) Metallic phases of cobalt-based catalysts in ethanol steam reforming: the effect of cerium oxide. Appl Catal A Gen 355:69–77
16. Song H, Ozkan U (2009) Ethanol steam reforming over Co-based catalysts: role of oxygen mobility. J Catal 261:66–74
17. Barroso MN, Gomez MF, Arrúa LA, Abello MC (2014) Co catalysts modified by rare earths (La, Ce or Pr) for hydrogen production from ethanol. Int J Hydrogen Energy 39:8712–8719
18. Sohn H, Ozkan US (2016) Cobalt-based catalysts for ethanol steam reforming: an overview. Energy Fuel 30:5309–5322
19. Turczyniak S, Teschner D, Machocki A, Zafeiratos S (2016) Effect of the surface state on the catalytic performance of a Co/CeO_2 ethanol steam-reforming catalyst. J Catal 340:321–330
20. Gaudillere C, González JJ, Chica A, Serra JM (2017) YSZ monoliths promoted with Co as catalysts for the production of H_2 by steam reforming of ethanol. Appl Catal A Gen 538:165–173
21. Kim KM, Kwak BS, YounghwanIm Park NK, Lee TJ, Lee ST, Kang M (2017) Effective hydrogen production from ethanol steam reforming using CoMg co-doped SiO2@$Co_{1-x}Mg_xO$ catalyst. J Ind Eng Chem 51:140–152
22. Sehested J (2006) Four challenges for nickel steam-reforming catalysts. Catal Today 111:103–110
23. Galetti AE, Gomez MF, Arrúa LA, Abello MC (2008) Hydrogen production by ethanol steam reforming over NiZnAl catalysts. Influence of Ce addition on carbon deposition. Appl Catal A Gen 348:94–102
24. Vizcaíno A, Arena P, Baronetti G, Carrero A, Calles J, Laborde M, Amadeo N (2008) Ethanol steam reforming on Ni/Al_2O_3 catalysts: effect of Mg addition. Int J Hydrogen Energy 33:3489–3492
25. Alberton AL, Souza MM, Schmal M (2007) Carbon formation and its influence on ethanol steam reforming over Ni/Al_2O_3 catalysts. Catal Today 123:257–264
26. Barroso MN, Galetti AE, Abello MC (2011) Ni catalysts supported over $MgAl_2O_4$ modified with Pr for hydrogen production from ethanol steam reforming. Appl Catal A Gen 394:124–131
27. Trane-Restrup R, Dahl S, Jensen AD (2013) Steam reforming of ethanol: effects of support and additives on Ni-based catalysts. Int J Hydrogen Energy 38:15105–15118
28. Chen X, Tadd A, Schwank J (2007) Carbon deposited on Ni/Ce–Zr–O isooctane autothermal reforming catalysts. J Catal 251:374–387
29. Song H, Ozkan U (2010) the role of impregnation medium on the activity of ceria-supported cobalt catalysts for ethanol steam reforming. J Mol Catal A Chem 318:21–29
30. Galetti AE, Barroso MN, Gomez MF, Arrúa LA, Monzón A, Abello MC (2012) Promotion of Ni/$MgAl_2O_4$ catalysts with rare earths for the ethanol steam reforming reaction. Catal Lett 142:1461–1469
31. Ho S-W, Su Y-S (1997) Effects of ethanol impregnation on the properties of silica-supported cobalt catalysts. J Catal 168:51–59
32. Sun S, Fujimoto K, Zhang Y, Tsubaki N (2003) A highly active and stable Fischer–Tropsch synthesis cobalt/silica catalyst with bimodal cobalt particle distribution. Catal Commun 4:361–364
33. Lucredio AF, Bellido JDA, Zawadzki A, Assaf EM (2011) Co catalysts supported on SiO_2 and γ-Al_2O_3 applied to ethanol steam reforming: effect of the solvent used in the catalysts preparation method. Fuel 90:1424–1430
34. Smith JS, Thrower PA, Vannice MA (1981) Characterization of Ni/SiO_2 catalysts by TEM, X-ray diffraction and chemisorption techniques. J Catal 68:270–285

35. Tarditi A, Barroso MN, Galetti AE, Arrúa LA, Cornaglia L, Abello MC (2014) XPS study of the surface properties and Ni particle size determination of Ni supported catalysts. Surf Interf Anal 46:521–529
36. Bengaard HS, Norskov JK, Sehested J, Clausen BS, Nielsen LP, Molenbroek AM, Rostrup Nielsen JL (2002) Steam reforming and graphite formation on Ni catalysts. J Catal 209:365–384
37. Chen D, Christensen KO, Ochoa Fernández E, Yu Z, Totdal B, Latorre N, Monzón A, Holmen A (2005) Synthesis of carbon nanofibers: effects of Ni crystal size during methane decomposition. J Catal 229:82–96
38. Koo KY, Lee S-H, Jung UH, Roh H-S, Yoon WL (2014) Syngas production via combined steam and carbon dioxide reforming of methane over Ni–Ce/$MgAl_2O_4$ catalysts with enhanced coke resistance. Fuel Process Technol 119:151–157
39. Luisetto I, Tuti S, Battocchio Ch, Lo Mastro S, Sodo A (2015) Ni/CeO_2–Al_2O_3 catalysts for the dry reforming of methane: the effect of $CeAlO_3$ content and nickel crystallite size on catalytic activity and coke resistance. Appl Catal A Gen 500:12–22
40. Löfberg A, Guerrero-Cavallero J, Kane T, Rubbens A, Jalowiecki-Duhamel L (2017) Ni/CeO_2 based catalysts as oxygen vectors for the chemical looping dry reforming of methane for syngas production. Appl Catal B 212:159–174
41. HSC Chemistry for Windows Software V 5.1. Outokumpu Research, Pori, Finland, 2003
42. Garbarino G, Riani P, Infantes-Molina A, Rodríguez-Castellón E, Busca G (2016) On Guido the detectability limits of nickel species on NiO/γAl_2O_3 catalytic materials. Appl Catal A Gen 525:180–189
43. Xu W, Liu Z, Johnston-Peck AC, Senanayake SD, Zhou G, Stacchiola D, Stach EA, Rodriguez JA (2013) Steam reforming of ethanol on Ni/CeO_2: reaction pathway and interaction between Ni and the CeO_2 support. ACS Catal 3:975–984
44. Galetti AE, Gomez MF, Arrua LA, Abello MC (2011) Ethanol steam reforming over Ni/$ZnAl_2O_4$–CeO_2. Influence of calcination atmosphere and nature of catalytic precursor. Appl Catal A Gen 408:78–86
45. Wang S, Lu CQ (1998) Reforming of methane with carbon dioxide over Ni/Al_2O_3 catalysts: effect of nickel precursor. Appl Catal A Gen 169:271–280
46. Gonzalez-De la Cruz VM, Holgado JP, Pereñiguez R, Caballero A (2008) Morphology changes induced by strong metal-support interaction on a Ni-ceria catalytic system. J Catal 257:307–314
47. Marjolein L, Toebes ML, Bitter JH, Jos van Dillen A, de Jong KP (2001) Impact of the structure and reactivity of nickel particles on the catalytic growth of carbón nanofibers. Catal Today 76:33–42
48. Vizcaíno AJ, Lindo M, Carrero A, Calles JA (2012) Hydrogen production by steam reforming of etanol using Ni catalysts base don ternary mixed oxides prepared by coprecipitation Int. J Hydrogen Energy 37:1985–1992
49. Zhang Ch, Li S, Li M, Wang S, Ma X, Gong J (2012) Enhanced oxygen mobility and reactivity for ethanol steam reforming. AIChE J 58:516–525
50. Trane-Restrup R, Dahl S, Jensen AD (2014) Steam reforming of ethanol over Ni-based catalysts: effect of feed composition on catalyst stability. Int J Hydrogen Energy 39:7735–7746
51. Bepari S, Basu S, Pradhan NC, Dalai AK (2017) Steam reforming of ethanol over cerium-promoted Ni–Mg–Al hydrotalcite catalysts. Catal Today 291:47–57
52. Santander JA, Tonetto GM, Pedernera MN, Lopez E (2017) Ni/CeO_2–MgO catalysts supported on stainless steel plates for ethanol steam reforming. Int J Hydrogen Energy 42:9482–9492
53. Hou Z, Gao J, Guo J, Liang D, Lou H, Zheng X (2007) Deactivation of Ni catalysts during methane auto thermal reforming with CO_2 and O_2 in a fluidized-bed reactor. J Catal 250:331–341
54. Corthals S, Van Nederkassel J, Geboers J, De Winne H, Van Noyen J, Moens B, Sels B, Jacobs P (2008) Influence of composition of $MgAl_2O_4$ supported $NiCeO_2ZrO_2$ catalysts on coke formation and catalyst stability for dry reforming of methane. Catal Today 138:28–32
55. Guo J, Lou H, Zhao H, Chai D, Zheng X (2004) Dry reforming of methane over nickel catalysts supported on magnesium aluminate spinels. Appl Catal A Gen 273:75–82
56. Nadini A, Pant KK, Dhingra SC (2005) K-, CeO_2- and Mn-promoted Ni/Al_2O_3 catalysts for stable CO_2 reforming of methane. Appl Catal A Gen 290:166–174
57. Sanchez-Sanchez MC, Navarro RM, Fierro JLG (2007) Ethanol steam reforming over Ni/M_xO_y–Al_2O_3 (M = Ce, La, Zr and Mg) catalysts: influence of support on the hydrogen production. Int J Hydrogen Energy 32:1462–1471
58. Natesakhawat S, Watson RB, Wang X, Ozkan US (2005) Deactivation characteristics of lanthanide-promoted sol-gel Ni/Al_2O_3 catalysts in propane steam reforming. J Catal 234:496–508